SCIENTIFIC REPORTS

OPEN

SUBJECT AREAS:
BIOLOGICAL SCIENCES
BIOLOGICAL MOLECULES
ENZYMES
ISOENZYMES

Received
19 October 2011

Accepted
16 December 2011

Published
27 January 2012

Correspondence and requests for materials should be addressed to S.A.E. (sharyn.endow@duke.edu)

Neck-motor interactions trigger rotation of the kinesin stalk

Hong-Lei Liu[1], Charles W. Pemble IV[2,3] & Sharyn A. Endow[1]

[1]Department of Cell Biology, Duke University Medical Center, Durham, NC 27710 USA, [2]Duke University X-ray Crystallography Facility, Duke University Medical Center, Durham, NC 27710 USA, [3]Duke Human Vaccine Institute, Duke University School of Medicine, Durham, NC 27710 USA.

Rotation of the coiled-coil stalk of the kinesin-14 motors is thought to drive displacements or steps by the motor along microtubules, but the structural changes that trigger stalk rotation and the nucleotide state in which it occurs are not certain. Here we report a kinesin-14 neck mutant that releases ADP more slowly than wild type and shows weaker microtubule affinity, consistent with defective stalk rotation. Unexpectedly, crystal structures show the stalk fully rotated – neck-motor interactions destabilize the stalk, causing it to rotate and ADP to be released, and alter motor affinity for microtubules. A new structural pathway accounts for the coupling of stalk rotation – the force-producing stroke – to changes in motor affinity for nucleotide and microtubules. Sequential disruption of salt bridges that stabilize the unrotated stalk could cause the stalk to initiate and complete rotation in different nucleotide states.

Kinesin motors hydrolyze ATP to produce force and move along microtubules or disassemble microtubules, regulating their dynamics in the cell. The mechanism by which the motors use ATP to perform work is still uncertain – a current hypothesis is that nucleotide binding or release causes small conformational changes in the motor that trigger the movement of a rigid structural element, resulting in a large displacement along a microtubule or removal of a tubulin dimer from a microtubule end[1]. For Ncd and other kinesin-14 motors, a large rotation of the α-helical coiled-coil stalk has been proposed to represent the force-producing stroke[2]. Studies of the related motor, myosin, have revealed a large rotation of the lever arm that constitutes the major mechanical component of the power stroke[3,4].

Displacements by the kinesin-14 motors are thought to be driven by rotation of the stalk, mediated by interactions of the end of the stalk – the neck – with the motor domain[2,5]. The step of ATP hydrolysis at which the stalk rotates has not been determined with certainty and is currently controversial. Single-motor laser-trap assays of the kinesin-14 motor Ncd have been interpreted to show that the stalk rotates when the motor binds to microtubules and releases ADP[5], but cryoEM studies of Ncd have led to the conclusion that the stalk rotates when the microtubule-bound motor binds ATP[6,7]. Two crystal structures have been reported that show the stalk of a kinesin motor in a rotated conformation. Both are structures of the Ncd motor without tubulin and show that stalk rotation is caused by ADP release[2,8]. Although ADP release appears to be capable of triggering stalk rotation, a different pathway of structural changes could occur when the motor binds to a microtubule. The structural changes should explain the changes in motor binding affinity for nucleotide and microtubules upon stalk rotation.

To obtain information about the structural changes that trigger stalk rotation and the nucleotide state in which the stalk rotates, we mutated the Ncd neck to alter stalk rotation. Analysis of the mutant motor shows microtubule-enhanced ATP hydrolysis, but slower ADP release and much lower affinity for microtubules than wild type. Although these properties indicate defective stalk rotation, crystal structures show the stalk fully rotated, promoted by previously unobserved neck-motor interactions that destabilize the unrotated stalk. These interactions are accompanied by structural changes that probably affect the water-mediated coordination of the bound nucleotide, causing ADP to be released. They also displace the C terminus of the motor, altering motor affinity for microtubules.

Results

Stalk-rotation mutant. The kinesin-14 motor Ncd exists as a dimer consisting of an N-terminal proline-rich, basic tail, α-helical coiled-coil stalk, and conserved motor domain with a short C terminus of 30 amino acids (Fig. 1A). The neck – the end of the stalk adjacent to the motor domain – forms a continuous coiled coil with the stalk in crystal structures[9,10]. Functional studies have demonstrated that the Ncd neck determines motor

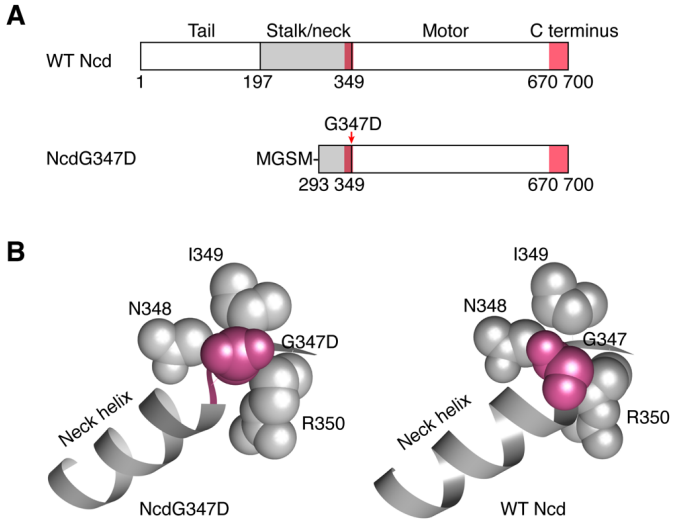

Figure 1 | NcdG347D. (A) WT (wild-type) Ncd is a dimer consisting of an N-terminal tail (M1-K196), α-helical coiled-coil stalk (gray, A197-R346) with neck (pink, R335-N348), and conserved motor domain (I349-S669) with a short C terminus (pink, C670-K700). The NcdG347D mutant was analyzed as a truncated dimeric protein (bottom; neck mutation, red arrow). (B) NcdG347D was designed based on potential steric effects of N348 and I349, and interactions with R350 that might stabilize the stalk in a different conformation. NcdG347D head H1 (left) (G347D, magenta); WT Ncd (right) (G347, magenta; PDB 2NCD).

directionality by biasing the direction of stalk movement[5,11]. Because of the importance of the neck in motor displacements or steps along microtubules, we mutated neck residue G347 to an aspartic acid to promote interactions with other residues that could sterically alter stalk movement. This change in the neck at the pivot point of stalk rotation is predicted to cause interactions with residues N348 and I349 that could either block or promote stalk rotation, or trap the stalk in an intermediate conformation (Fig. 1B). In addition, ionic interactions of the mutated residue with R350 could stabilize the stalk in an unrotated, fully rotated, or partially rotated conformation. A change in the ability of the stalk to rotate is expected to alter ADP release by the motor and motor binding to microtubules. A truncated dimeric NcdG347D protein was expressed and purified, and tested for ADP release and microtubule binding in biochemical assays.

Motor-microtubule interactions. We tested NcdG347D in single-turnover ADP release assays to determine if the mutant could bind and release nucleotide. The mutant and wild-type Ncd were incubated with fluorescently-labeled mant-ATP for ≥1.5 hr to overnight to allow the motors to bind the nucleotide and hydrolyze the bound nucleotide to ADP, then unlabeled ATP was added to replace the ADP, promoting ADP release. Mant-nucleotide fluorescence is enhanced by binding to proteins; thus, the starting fluorescence levels in these assays are a measure of nucleotide binding by the motor. A decrease in fluorescence is observed when bound mant-ADP is released from the motor. The levels of motor-mant-ADP fluorescence at the start of the assays were similar for NcdG347D and wild-type Ncd, indicating that the mutant is capable of binding nucleotide (Fig. 2A). Upon addition of ATP, 0.5 μM NcdG347D released mant-ADP with a rate constant (mean±SEM, 0.00109±0.00001 s^{-1}, n=6) that was slightly, but significantly lower than wild type (0.00164±0.00001 s^{-1}, n=6). Assays with 1 μM motor again gave a significantly lower rate constant for NcdG347D than wild type. The assays showed that the G347D mutant can bind and release nucleotide, but the rate of ADP release is ~0.7 times slower than wild type, indicating a possible defect in stalk rotation.

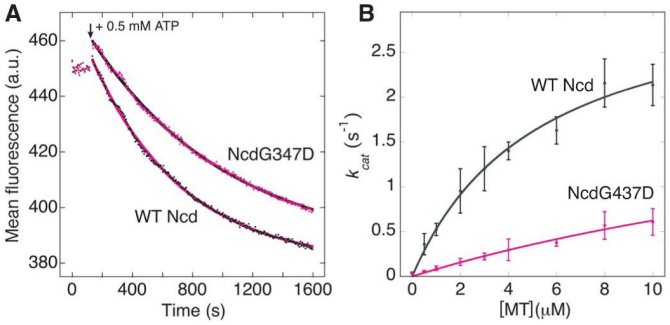

Figure 2 | NcdG347D kinetic assays. (A) ADP release assays. Mean fluorescence (n=6) versus time after adding 0.5 mM ATP (arrow) to 0.5 μM NcdG347D (magenta; curve fit, black) or WT Ncd (black; curve fit, magenta) bound to fluorescently-labeled mant-ADP. a.u., arbitrary units; s, seconds. (B) ATPase assays. k_{cat} (s^{-1}) versus [MT] ([tubulin dimer]) fit to the Michaelis-Menten equation. Assays without microtubules, k_{cat} at [MT]=0, give the basal ATPase rate constant. NcdG347D, magenta (n=3); WT Ncd, black (n=3); mean±SEM. MT, microtubule.

Motor-microtubule pelleting assays were performed to test NcdG347D binding affinity for microtubules. The assays showed NcdG347D in the pellet even without microtubules, presumably caused by aggregation due to the high motor concentrations required for these assays. This was also observed for wild-type Ncd, tested as a control. The amount of motor that pelleted without microtubules was too high to obtain reliable dissociation constants of the motor from microtubules using these assays.

Microtubule gliding assays were performed to determine whether NcdG347D motors bound to a glass surface could support microtubule binding and gliding. Ensemble gliding assays with ATP showed no microtubules bound to the motor attached to a coverslip surface (3 assays, total=4) or partially bound microtubules that did not move (1 assay), using ~10-fold higher microtubule concentrations than for wild type. Partially bound microtubules that did not move were observed under the conditions of our assays even after adding >2-fold more NcdG347D motor than in assays of wild type. Under the same conditions, Wild-type Ncd showed good microtubule motility (>90% of bound microtubules moved, n=76) with a velocity of 7.0±0.1 μm/min (n=32), comparable to previously reported velocities[12].

Motility assays of the NcdG347D motor without added ATP showed tangles of bundled and clumped microtubules and some regions of single immobile microtubules, indicating that the motor is capable of binding to and cross-linking microtubules in rigor. Nucleotide-sensitive microtubule binding indicates that the assays contain active NcdG347D motors, rather than "dead" or inactive motors that do not bind microtubules, or bind microtubule in rigor even in the presence of ATP. Despite this, the poor binding of microtubules to the coverslip surface in assays with ATP indicates that the NcdG347D motor binds weakly to microtubules compared to wild type.

We then tested the NcdG347D mutant in steady-state ATPase assays to determine the effect of the motor on ATP hydrolysis with and without microtubules. These assays were also performed because they can yield estimates of differences in motor affinity for microtubules compared to wild type. Assays without microtubules showed a basal ATPase rate constant for NcdG347D (0.033±0.003 s^{-1}, n=3) that was ~0.8 times lower than wild-type Ncd (0.042±0.007 s^{-1}, n=3), similar to the ~0.7 times lower NcdG347D mant-ADP release rate constant relative to wild type, although the basal values overlap when the experimental error is taken into account. Assays with microtubules showed stimulation of the NcdG347D basal ATPase activity with a $K_{m,MTs}$ (30±15 μM, n=3) ~6-fold higher than wild type (5.3±0.9 μM, n=3), indicating much lower microtubule

affinity (Fig. 2B). The data demonstrate that the NcdG347D neck mutation affects motor affinity for microtubules. The higher $K_{m,MTs}$, together with the lower ADP release rate constant, imply that the G347D mutation interferes with rotation of the stalk, reducing the motor ADP release rate and its affinity for microtubules.

NcdG347D crystal structure. To determine the structural effects of the NcdG347D neck mutation on stalk rotation, we crystallized the motor and solved the structure. Despite the evidence for defective stalk rotation, crystals of the NcdG347D motor grown under different conditions showed the stalk and one head, H1, rotated relative to the other head, H2, or wild-type Ncd (Fig. 3A). The new structure, solved to 2.34 Å resolution (Table 1 and Supplementary Fig. 1), differs markedly from previous Ncd dimer structures that show the two heads related by two-fold symmetry to the coiled-coil stalk (Fig. 3B), representing the motor-ADP free in solution[9,10,13]. It is similar to the previously reported stalk-rotated Ncd structures[2,8] in the large ~75° angle change of the stalk (Fig. 3A and Supplementary Fig. 2). One of the heads, H1, of NcdG347D and the previous stalk-rotated structures retains the same relationship to the stalk as the stalk-unrotated motor-ADP, but the other head, H2, is asymmetrically positioned relative to the stalk and head H1, due to the rotation of the stalk with the attached head H1 (Fig. 3B and Supplementary Movies 1 and 2).

The stalk-rotated conformation has been proposed to resemble the motor bound by one head, H2, to a microtubule, and is thought to

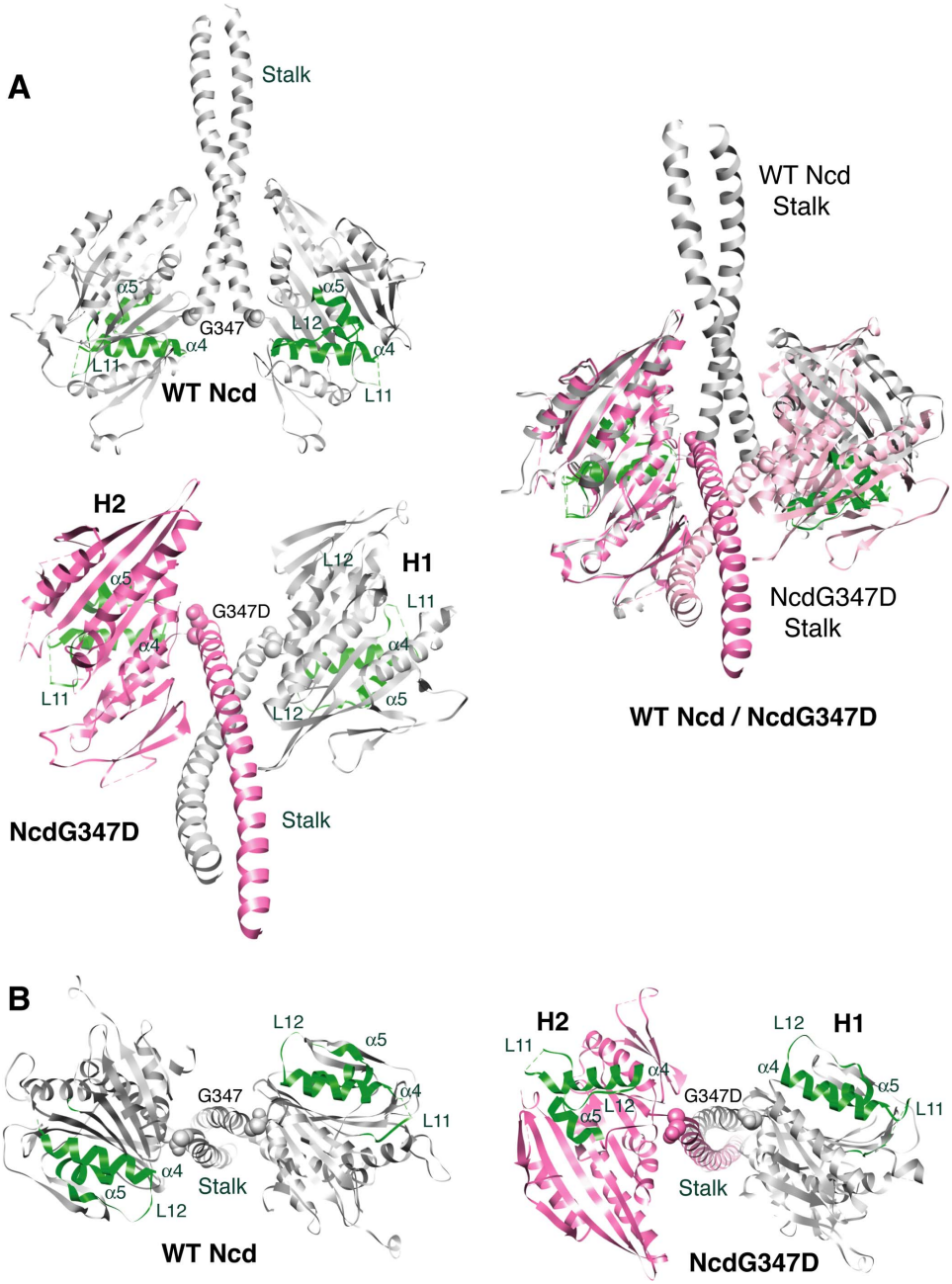

Figure 3 | NcdG347D stalk-rotated conformation. (A) The NcdG347D stalk and head H1 are rotated relative to head H2 (bottom) or WT Ncd (top). NcdG347D head H2 (left) is shown aligned with the WT Ncd head to the left. Superposing the two models (right) shows the large, ~75° angle change of the NcdG347D stalk and H1. (B) WT Ncd heads show two-fold symmetry with respect to the coiled-coil stalk (left); NcdG347D head H2 is asymmetrically positioned relative to the stalk and H1, due to the rotation of the stalk and H1 (right). NcdG347D chain A (H1), gray or pink; chain B (H2), magenta; G347D, space-filled. WT Ncd, PDB 1CZ7; G347, space-filled. Switch II (L11-α4-L12-α5), green.

Table 1 | NcdG347D x-ray diffraction data and refinement statistics

X-ray diffraction data	
Space group	C2
Cell dimensions: a, b, c (Å)	160.5, 67.1, 94.4
α, β, γ (°)	90.0, 98.9, 90.0
Resolution (Å)	46.6–2.34 (2.40–2.34)
R_{sym}	0.07 (0.43)
$I/\sigma I$	22.70 (1.92)
Completeness (%)	86.9 (59.3)
Redundancy	5.9 (4.1)
Refinement	
Resolution (Å)	46.6–2.34
Total measured reflections	215,426
Unique reflections	36,362 (1,229)
R_{work}/R_{free}	0.216/0.250
Atoms: protein (chain A)/protein (chain B)/Mg^{2+}/ADP/water/glycerol	5,715/5,484/1/78/122/70
B factors: chain A/chain B/Mg^{2+}/ADP (chain A, H1)/ADP (chain B, H2)/glycerol/water	60.6/82.4/50.8/48.9/71.6/77.4/48.0
Rmsd bond length (Å)	0.004
Rmsd bond angles (°)	0.759
Ramachandran analysis: favored/allowed/disallowed (%)	96.93/99.85/0.15

Values in parentheses are for the highest resolution shell.

represent the post-powerstroke conformation of the motor[2,8]. Because head H1 retains the same extensive interactions with the stalk as in the wild-type motor, or motor-ADP, it can be thought of as being in the pre-stroke conformation, while H2 is in the post-stroke conformation[14]. Thus, the two heads of stalk-rotated Ncd structures represent different states of the motor with respect to the force-producing stroke.

Strikingly, the NcdG347D crystal structure differs from the two previous stalk-rotated models in that head H2, the head that interacts with the microtubule in dockings of a stalk-rotated Ncd structure into motor-microtubule cryoEM density maps[2], shows previously unobserved interactions of the neck with loop L13 (Fig. 4). G347D is hydrogen-bonded to S639 of loop L13, tilting loop L13 towards the neck and changing its angle by ~40° compared to L13 in NcdG347D head H1, which is oriented similarly to L13 in head H1 of previous stalk-rotated Ncd structures. NcdG347D also shows changes in the position of L13 in head H2 relative to wild-type Ncd (Supplementary Movie 2); this is also true of the previous stalk-rotated Ncd structures (Supplementary Movies 3 and 4), but the movements of L13 are more pronounced in NcdG347D head H2. The interactions of G347D with S639 in head H2 disrupt the dipole-charge bond between neck residue N340 and loop L13 residue K640 – this results in rotation of the NcdG347D stalk, since disrupting N340-K640 interactions has been shown to cause the stalk to rotate[2,5]. R350, which is positioned near S639 because of the change in angle of loop L13, hydrogen bonds to both S639 and N340, stabilizing the stalk-rotated conformation (Fig. 4). The G347D mutated neck residue thus promotes stalk rotation by disrupting the N340-K640 interaction and stabilizes the stalk-rotated conformation by allowing R350 to hydrogen bond to N340, preventing the N340-K640 bond from reforming.

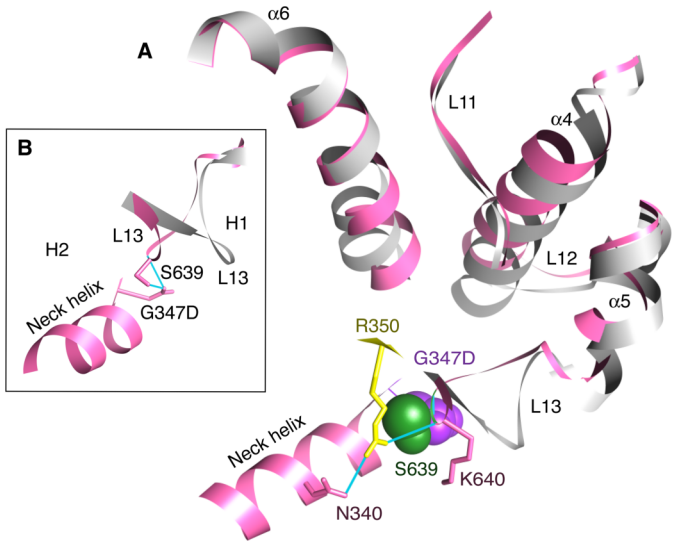

Figure 4 | NcdG347D neck-motor interactions. (A) G347D in head H2 (purple, space-filled) is hydrogen bonded to S639 of loop L13 (green, space-filled), tilting L13 towards the stalk/neck by ~40° compared to head H1 (B). This disrupts N340–K640 neck-motor interactions, causing the stalk to rotate. R350 (yellow) hydrogen bonds (cyan) to S639 of loop L13 and neck residue N340, stabilizing the stalk-rotated conformation. The microtubule-binding elements of head H2 (magenta), L11-α4-L12-α5, are displaced laterally slightly relative to head H1 (gray), indicating a difference in nucleotide state between the heads.

The microtubule-binding structural elements of NcdG347D head H2, switch II L11-α4-L12-α5, are displaced laterally slightly relative to head H1 (Fig. 4) or wild-type Ncd (Supplementary Movie 2), but the difference in tilt of helices α4 and α5 is not as great as between kinesin motors in the ATP versus ADP states[15,16]. The slight lateral displacement indicates a difference in nucleotide state between the two heads, which have been interpreted to represent an ADP state (H1) and transition towards a no-nucleotide state (H2)[2].

The NcdG347D structure also shows the C terminus of the motor following K671 near the end of helix α6, which was seen for the first time in NcdT436S (PDB 3L1C), a recently reported stalk-rotated Ncd crystal structure, in which residues are visible to K674 in head H2[8]. The C terminus of head H2 in our new NcdG347D structure has been modeled only to T673 (Fig. 5), although density is visible that can be attributed to residues following T673 (Supplementary Fig. 3). The visible C-terminus residues in head H2 undergo a large change in position relative to wild-type Ncd, accompanied by movement of loop L2 (Supplementary Movies 2 and 4). The modeled region of the NcdT436S C terminus folds into a structure resembling the kinesin-1 neck linker[8], as reported previously for the kinesin-14 KCBP[17], and has been proposed to stabilize the ATP conformation of the kinesin-14 motors[17].

Notably, the NcdG347D C terminus diverges in trajectory from NcdT436S, caused by the interactions of G347D with S639 of loop L13 that change the angle of the loop, tilting it toward the neck (Fig. 5). This moves the loop close to the C terminus, causing loop

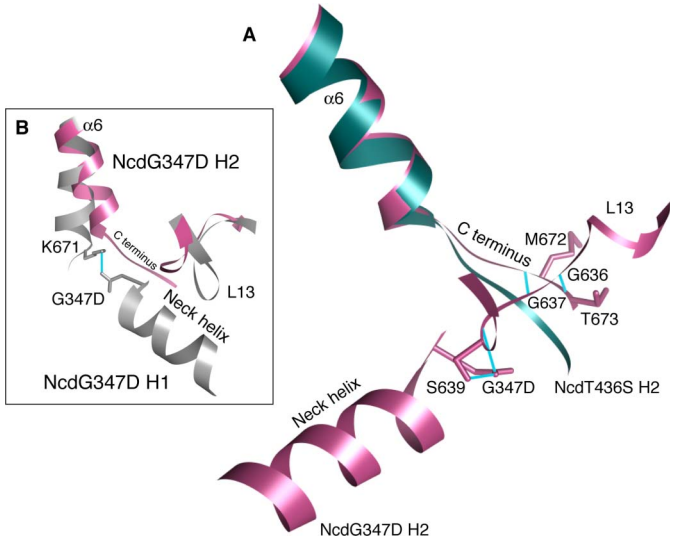

Figure 5 | NcdG347D C terminus. (A) NcdG347D versus NcdT436S C terminus. The modeled residues following helix α6 of NcdG347D head H2 (magenta) differ in trajectory from NcdT436S (dark cyan), where the C-terminus residues after K671 were first observed. The change in angle of loop L13 causes NcdG347D C terminus residues M672 and T673 to hydrogen bond (cyan) to G637 and G636 of L13, respectively, altering the position of the C terminus of head H2. (B) C terminus of NcdG347D head H1 versus H2. The mutated G347D residue in head H1 hydrogen bonds (cyan) to K671, displacing the C terminus of head H1 (gray). Head H2, magenta.

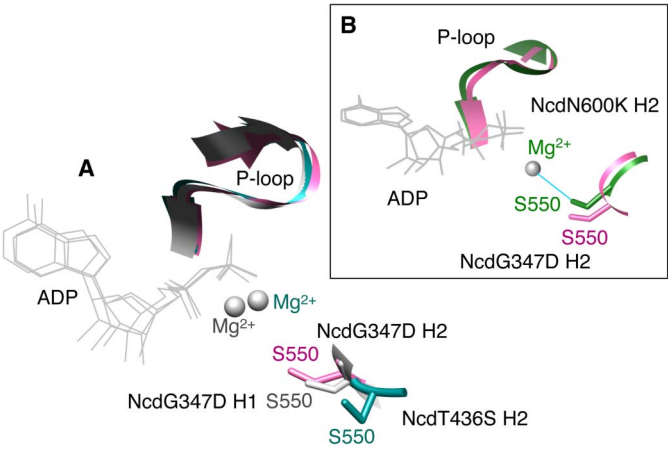

Figure 6 | NcdG347D active site. (A) Switch I residue S550 has moved closer to the bound ADP in NcdG347D head H2 (magenta) compared to H1 (gray). S550 in NcdT436S head H2 (dark cyan) is displaced relative to S550 in both NcdG347D head H1 and H2. ADP in NcdG347D head H2 is unstable compared to H1 (Supplementary Fig. 4) and NcdT436S releases ADP 10-fold faster than wild-type Ncd without microtubules, correlating the switch I movements with ADP release. (B) NcdG347D versus NcdN600K. S550 of NcdG347D head H2 is positioned similarly to S550 of NcdN600K head H2 (dark green), which hydrogen bonds (cyan) to the Mg^{2+}, causing ADP to be released.

L13 residues G636 and G637 to hydrogen bond to C terminus residues T673 and M672, respectively, displacing the C terminus relative to its position in the NcdT436S model. The angle of divergence of ~15° and the position of the last modeled NcdG347D residues indicate that the following twenty-seven C terminus residues are probably displaced relative to the NcdT436S C terminus.

This is also true of NcdG347D head H1, where the mutated G347D neck residue is hydrogen bonded to K671, one of the last visible residues of the chain (Fig. 5B); this probably displaces the C terminus in head H1, as well as head H2. The Ncd C terminus is critically important for microtubule binding – its deletion causes failure by the motor to bind microtubules to the coverslip in motility assays[11]. The much lower microtubule affinity of NcdG347D compared to wild type is most likely caused by the displacement of the motor C terminus.

Nucleotide is bound to the active site of both heads (Fig. 6 and Supplementary Fig. 4), but there is slightly reduced density for the nucleotide in head H2 and missing density for several water molecules that coordinate the nucleotide and Mg^{2+} in head H1, indicating instability of the ADP in H2. The active site of head H2 contains density near the β-phosphate of ADP that approximates the position of Mg^{2+} (Supplementary Fig. 4A, arrow), but differs from its position in head H1 and refines poorly when Mg^{2+} is modeled into the density. The Mg^{2+} in head H2 was therefore omitted from the final model. ADP has been built into the density in H2, and ADP and Mg^{2+} in H1, both coordinated by water molecules, as reported previously[16,18]. The ADP, Mg^{2+} and waters, in turn, are coordinated by nearby motor residues. NcdN600K head H2 interacts with the microtubule when the stalk-rotated motor is docked into motor-microtubule cryoEM maps[2] and head H2 of both NcdN600K and NcdT436S shows reduced density for ADP compared to H1, indicating that ADP release occurs with stalk rotation[2,8]. The lower density corresponding to the nucleotide and missing density for water molecules that coordinate the bound nucleotide and Mg^{2+} in NcdG347D head H2 implies that ADP is also released from NcdG347D head H2 upon stalk rotation, despite its lower basal rate constant for release in kinetic assays.

The NcdG347D model shows a structural change between the two heads involving switch I that has not been reported previously – in head H2, switch I residue S550 has moved closer to the bound ADP compared to H1 (Fig. 6). The position of S550 in NcdG347D head H2 is close to that in NcdN600K head H2 (PDB 1N6M; Fig. 6B). In NcdN600K, S550 forms a hydrogen bond to the Mg^{2+}, disrupting its coordination and causing release of the bound ADP. S550 is disordered in head H1 of NcdT436S, a motor that releases ADP 10-fold faster than wild type without microtubules, and head H2 of NcdT436S shows S550 displaced even further than in NcdG347D head H2 (Fig. 6A), correlating movement of switch I residue S550 with ADP release. The movements of S550 and other switch I residues in NcdG347D head H2 probably affect the waters coordinating the ADP and Mg^{2+}, resulting in ADP release upon stalk rotation.

Discussion

Force production by the kinesin motors is hypothesized to involve small movements of the motor that are amplified by a large conformational change of a rigid structural element, coupled to changes in motor binding affinity for nucleotide and microtubules[1]. For the kinesin-14 motors, rotation of the coiled-coil stalk is thought to represent the force-producing stroke[2], but the structural changes that trigger stalk rotation and the nucleotide state in which it occurs have been uncertain. Mutants can reveal interactions of the wild-type motor by stabilizing normally transient or unstable states. Because force production by the kinesin-14 motors is expected to affect displacements or steps along the microtubule, in which the neck plays an important role[5,11], we mutated the neck residue at the end of the kinesin-14 Ncd stalk, G347, to an aspartic acid to alter stalk rotation. The mutated neck residue was expected to block or promote stalk rotation, or cause the stalk to assume a partially rotated conformation. Altered stalk rotation would affect ADP release and motor binding affinity for microtubules; e.g., slower ADP release than wild type and weaker microtubule binding would imply defective rotation of the stalk.

Analysis of the NcdG347D neck mutant showed that the motor can bind to and release nucleotide and that ATP hydrolysis is stimulated by microtubules. However, ADP release is slower than wild type and motor affinity for microtubules is much weaker, consistent with defective stalk rotation. Unexpectedly, the NcdG347D motor, crystallized under different conditions, shows the stalk fully rotated, in a conformation similar to two previously reported Ncd mutants[2,8], but with previously unobserved structural changes. The new structural changes identify residue interactions that lead to stalk rotation and its probable nucleotide state – they implicate neck-motor interactions in triggering stalk rotation, coupled to ADP release and changes in motor affinity for microtubules, and imply that the stalk initiates and completes rotation in different nucleotide states.

The stalk-rotated NcdG347D structure most likely represents an unstable or transient state of the wild-type motor that is stabilized by interactions of the mutated neck residue. It shows three previously unobserved structural changes that identify residue interactions and structural changes that probably occur in the wild-type motor. The first is the interaction of the mutated residue with loop L13, which tilts the loop towards the neck, disrupting N340-K640 interactions, causing the stalk to rotate[2,5]. Transient interactions of the G347 residue with loop L13 probably occur in wild-type Ncd, leading to disruption of the N340-K640 bond, triggering stalk rotation. The interactions of G347D with loop L13 cause R350 to hydrogen bond to S639 of L13 and to N340 of the neck, stabilizing the stalk-rotated conformation and preventing the N340-K640 bond from reforming. The second change involves switch I, a motif first identified in the G-proteins and conserved in the kinesins and myosins, that undergoes large conformational changes upon nucleotide exchange. Switch I residue S550 moves closer to the bound ADP, undergoing movements that are most likely accompanied by other switch I residues, consistent with the disordered structure of this region. These movements probably affect the water-mediated coordination of nucleotide and Mg^{2+}, causing ADP release from head H2 upon stalk rotation.

The third large change is at the motor C terminus. Strikingly, NcdG347D C terminus residues beyond K671 near the end of helix α6 are visible in head H2 that have been seen only once before, in a recently reported stalk-rotated Ncd crystal structure, NcdT436S[8]. The modeled residues fold into a conformation that resembles the neck-linker of kinesin-1, which, together with the cover strand[19], is thought to be the primary force-producing mechanical element of the motor[20,21]. However, the C terminus of NcdG347D head H2 is displaced relative to NcdT436S because of its interactions with the tilted loop L13. This probably displaces the residues beyond the end of the last modeled residue, which are essential for motor binding to microtubules[11]. Displacement of the NcdG347D C terminus would explain the much weaker affinity of the mutant for microtubules compared to wild type. This effect is similar to the kinesin-14 AtKCBP, in which dislodging of the analogous C-terminus region, the neck mimic, by binding of the following helix to a Ca^{2+}-bound calmodulin-like regulatory protein, KIC, disrupts motor-microtubule interactions[22].

The weak affinity of the NcdG347D motor for microtubules might represent a transient state of the wild-type motor that occurs during stalk rotation. Changes in microtubule binding affinity occur when wild-type Ncd interacts with microtubules; these changes could be caused by movements of the C terminus, induced by neck-motor interactions and stalk rotation. Stabilization of the movements might occur only upon binding by the C terminus to the correct site on the microtubule.

NcdG347D and the previously reported stalk-rotated mutants, NcdN600K and NcdT436S[2,8], are complexed with ADP, rather than ATP, with reduced density in head H2, the head that does not rotate with the stalk. This implies that stalk rotation occurs in the mutants at a step of the cycle prior to ATP binding, associated with ADP release from the rotated head, rather than upon ATP binding. ADP release by NcdN600K and NcdT436S has been proposed to trigger stalk rotation by destabilizing the unrotated motor conformation, causing structural changes that lead to stalk rotation.

In NcdN600K, the mutated residue moves towards switch I and forms a hydrogen bond to R552 of switch I, which causes S550 of switch I to hydrogen bond to the Mg^{2+} at the active site, destabilizing the bound ADP[2]. Movement of N600K and R552 towards each other weakens N340-K640 neck-motor interactions, causing the stalk to rotate. By contrast, the mutated residue in NcdT436S hydrogen bonds with a water molecule in the nucleotide-binding cleft that has moved relative to wild type[8]. This interaction might result in the large change in position of the S550 switch I residue that we observe here, destabilizing the water-mediated coordination of the bound Mg^{2+} and causing ADP release. This would account for the much faster ADP release by the NcdT436S motor compared to wild type[8]. The structural changes caused by ADP release by NcdT436S that lead to stalk rotation are not certain from the crystal structure, largely because of the disordered regions in the model. One possibility is that the movement of switch I S550 and other switch I residues destabilizes N340-K640 neck-motor interactions, as proposed for N600K-R552 interactions in NcdN600K.

The NcdG347D crystal structure identifies structural elements involved in stalk rotation – the G347 neck residue and loop L13 – that differ from those implicated by the two previous mutants. It also indicates structural mechanisms by which stalk rotation could be coupled to ADP release and changes in motor affinity for microtubules through movements of switch I and interactions of loop L13 with the motor C terminus, respectively, explaining the changes that occur when wild-type Ncd binds to a microtubule and releases ADP.

The NcdG347D crystal structure, as well as the two previous stalk-rotated Ncd crystal structures, shows that stalk rotation does not require microtubule binding. The two heads of stalk-unrotated Ncd and head H1 of stalk-rotated structures are stabilized by an extensive network of interactions between the neck and motor domain that include three or more salt bridges and a dipole-charge interaction between neck residue N340 and K640 of loop L13[8,9]. These bonds between the stalk and one of the heads must be disrupted to allow the stalk to rotate. The Ncd crystal structures that show the stalk fully rotated even in the absence of microtubules are caused by structural changes in the mutants that destabilize the N340-K640 bond. Without microtubules, the stalk rotates, due to destabilization of the key N340-K640 bond by interactions of the mutated residue with other residues. In the presence of microtubules, motor-microtubule interactions cause structural changes in the motor that lead to stalk rotation and ADP release.

The structural changes in wild-type Ncd, induced by interactions of the motor with microtubules, are likely to involve interactions of the same structural elements as in the NcdG347D motor. The changes probably involve sequential disruption of the network of salt bridges between the neck and motor that stabilize Ncd in an unrotated conformation. Weak binding interactions between the motor and microtubule could partially disrupt these bonds in the Ncd·ADP·MT state, initiating stalk rotation and the movement of switch I residues, resulting in ADP release, forming the Ncd-MT state (Fig. 7). ATP binding could then cause G347 to interact transiently with loop L13, disrupting the N340-K640 dipole-charge interaction, causing the stalk to rotate fully and altering motor affinity for microtubules, forming Ncd·ATP·MT. This hypothesis is consistent with the proposal from recent FRET studies that the Ncd stalk rotates in two nucleotide states in the presence of microtubules – it initiates movement when the motor binds to a microtubule and releases ADP, and completes rotation upon ATP binding[23].

The NcdG347D motor provides new insights into the residue interactions and structural changes that trigger stalk rotation and the most probable nucleotide states in which it occurs. Studies that trap further intermediates in this structural pathway should provide

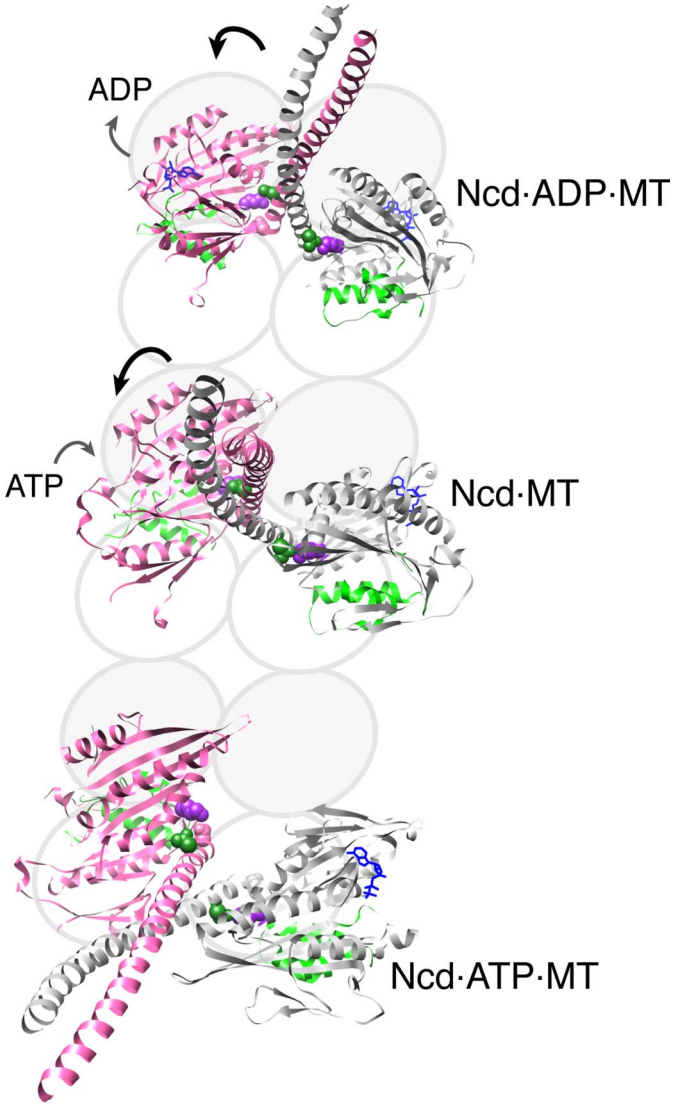

Figure 7 | Model for Ncd stalk rotation. Ncd-ADP (ADP, blue) interactions with a microtubule (MT, gray-white; plus end, top) result in weakly bound Ncd-ADP-MT (top). The weak-binding interactions induce structural changes that disrupt salt bridges between the neck and head H2 (magenta), initiating stalk rotation (black arrow) and ADP release, forming Ncd-MT (center). ATP binding to the microtubule-bound head results in neck-L13 interactions, disrupting the N340-K640 bond (space-filled, dark green-purple), causing the stalk to rotate fully, forming Ncd-ATP-MT (bottom). Crystallization of NcdG347D with the stalk fully rotated is caused by interactions of the mutated residue that disrupt the N340-K640 bond, triggering stalk rotation. The NcdG347D structural changes imply that ADP release follows initiation of stalk rotation, whereas ADP release by NcdN600K and NcdT436S is interpreted to cause the stalk to rotate.

a fuller understanding of the mechanism leading to stalk rotation and force production by the kinesin motors. This large conformational change is critically important to motor function - it is thought to represent the force-producing stroke of the kinesin-14 motors and is probably paralleled by a large movement of the neck linker bound to the cover strand in kinesin-1 and kinesins of other groups. The underlying events that lead to stalk rotation are anticipated to shed light on the mechanism of energy transduction by the motors.

Methods

Plasmids and proteins. Plasmids for expression of truncated wild-type Ncd and NcdG347D proteins (MGSM-H293-K700; Fig. 1) were constructed using conventional methods and a modified *pET* expression plasmid, *pMW172*[24]. Proteins were expressed in *Rosetta2 (DE3) pLysS* host cells (Novagen), which also express tRNAs for seven rarely used *E. coli* codons. Purification was by SP-Sepharose chromatography followed by Superose 12 FPLC, as described previously[25]. NcdG347D protein from a plasmid with the C-terminal 26 codons optimized for *E. coli* expression (sequence available on request) was also tested for crystallization. Crystals grown under previous conditions[2] appeared overnight and diffracted, as for protein from a plasmid with a non-optimized C terminus, but the protein expressed with an optimized C terminus was not tested for crystallization under the new conditions (see below) because it did not appear to behave significantly differently. The NcdG347D structure reported here is from protein expressed with a non-optimized C terminus.

ADP release assays. Single-turnover ADP release assays were performed in HEM50 (HEM=10 mM HEPES pH 7.2, 1 mM $MgCl_2$, 1 mM EGTA; HEM50=HEM + 50 mM NaCl) by incubating 0.5 or 1 μM purified motor with 4-fold excess mant-ATP (2'(3')-O-(N-methyl-anthraniloyl)-adenine 5'-triphosphate) for 5–10 min at RT, then ≥1.5 hr to overnight on ice in the dark. Fluorescence (λ_{ex}=356 nm, λ_{em}=446 nm) was read for 120 s at 22°C in a Varian Cary Eclipse fluorimeter to establish a baseline, then continued to 1600 s after manually adding 0.5 mM Mg·ATP. Data were averaged and fit to $y=m3+m2*e^{-m1*M0}$, where y=fluorescence at M0=time (s), m2=total fluorescence decrease, m3=fluorescence at t=∞ and m1=k_{off}. A small jump in fluorescence, evident in the mean curves, sometimes occurred upon addition of ATP and was attributed to perturbation of the reaction mix during nucleotide addition.

Microtubule pelleting assays. Purified wild-type and mutant proteins were incubated with microtubules in HEM50; bound and unbound motor were separated by ultracentrifugation and analyzed by SDS-PAGE, as described[26].

Motility assays. NcdG347D was expressed as a glutathione S-transferase (GST) fusion protein (GST/NcdK210-K700) for motility assays[27] with the corresponding wild-type Ncd protein (GST/MC1)[12] as a control. Motility assays were performed using proteins partially purified by SP-Sepharose chromatography and anti-GST antibodies to attach the motors to the glass surface. Relative concentration of the wild-type and mutant GST/Ncd motors was estimated by OD_{280} and SDS-PAGE.

ATPase assays. Steady-state basal ATPase assays were performed using FPLC-purified proteins and a pyruvate kinase/lactate dehydrogenase-coupled NADH oxidation reaction[26]. Controls with ADP were performed prior to each assay to ensure that the decrease in OD_{340} was linear with increasing ADP concentration over the assay time.

Crystallization and structure determination. NcdG347D was crystallized by adding purified motor in HEM300 (HEM + 300 mM NaCl) + Mg·ATP to the well solution in a 1 : 1 ratio. A screen for new crystallization conditions was performed and crystals were also grown under previous conditions[2]. Both conditions gave crystals with the C2 space group and the same unit cell, and the models from both conditions showed NcdG347D with a rotated stalk, but R_{free} and R_{work} for the crystals grown under the previous conditions did not fall during the refinement, indicating that there was a problem with the data or the model. The new conditions produced the NcdG347D structure reported here. Crystals were grown in sitting drops containing 4.5 mg/ml motor + 2 mM Mg·ATP and well solution of 10% PEG 3350, 20 mM Na_2SO_4, 0.1 M Tris-Bis-Propane, pH 6.5 at 15°C. Crystals were frozen in well solution + 25% glycerol as a cryoprotectant and stored in liquid nitrogen. Diffraction data were collected on the 22-BM beamline at the Advanced Photon Source, Argonne National Laboratory. Crystals contained one dimer in the asymmetric unit. The structure was solved by molecular replacement using a previous stalk-rotated Ncd crystal structure as a search model (PDB 1N6M). Diffraction data were indexed and scaled to 2.34 Å with HKL2000[28], optimizing resolution at the expense of completeness (Table 1, 86.9% (59.3%)), given that the statistics for the highest resolution shell were good ($I/\sigma I$=~2, redundancy=~4). Scaling the data to lower resolution (2.74 Å) and higher completeness (98.0% (85.7%)) produced a model after refinement (R_{work}/R_{free}=0.214/0.249) that was the same quality as the 2.34 Å model (Table 1, R_{work}/R_{free}=0.216/0.250) and almost identical to the 2.34 Å model (overall rmsd=0.155 Å). The 2.74 Å model also showed only slight differences from the 2.34 Å model in the composite omit electron density at the regions of interest – the site of mutation and the active site (Supplementary Fig. 1). Because the two models do not differ significantly in quality and are almost identical, the interpretations we report here are from the 2.34 Å model. Iterative refinement was performed with PHENIX[29]; the model was manually rebuilt with COOT[30] and validated with MolProbity[31]. A Ramachandran plot showed 99.85% of residues in the favored or allowed regions and one residue, G347D of head H1, in the outlier region. Examination of the modeled G347D residue showed that it fit well into the observed electron density (Supplementary Fig. 1). X-ray data collection and refinement statistics are given in Table 1. Residues missing in the refined model are chain A residues 385-391, 518, 542–546, 588–596, 673–700 and chain B residues 385–387, 494–512, 540–547, 588–597, 674–700. Figures and animations were made with Chimera[32], except for Supplementary Fig. 1, 3 and 4, which were made in PyMol[33].

Coordinates and structure factors for the 2.34 Å model have been deposited in the Protein Data Bank under accession code 3U06.

1. Howard, J. *Mechanics of motor proteins and the cytoskeleton.* 1st edn, (Sinauer Associates, Inc., 2001).
2. Yun, M. *et al.* Rotation of the stalk/neck and one head in a new crystal structure of the kinesin motor protein, Ncd. *EMBO J.* **22**, 5382–5389 (2003).
3. Rayment, I. *et al.* Three-dimensional structure of myosin subfragment-1: a molecular motor. *Science* **261**, 50–58 (1993).
4. Dominguez, R., Freyzon, Y., Trybus, K. M. & Cohen, C. Crystal structure of a vertebrate smooth muscle myosin motor domain and its complex with the essential light chain: visualization of the pre-power stroke state. *Cell* **94**, 559–571 (1998).
5. Endow, S. A. & Higuchi, H. A mutant of the motor protein kinesin that moves in both directions on microtubules. *Nature* **406**, 913–916 (2000).
6. Wendt, T. G. *et al.* Microscopic evidence for a minus-end-directed power stroke in the kinesin motor ncd. *EMBO J.* **21**, 5969–5978 (2002).
7. Endres, N. F., Yoshioka, C., Milligan, R. A. & Vale, R. D. A lever-arm rotation drives motility of the minus-end-directed kinesin Ncd. *Nature* **439**, 875–878 (2006).
8. Heuston, E., Bronner, C. E., Kull, F. J. & Endow, S. A. A kinesin motor in a force-producing conformation. *BMC Struct. Biol.* **10**, 19 (2010).
9. Sablin, E. P. *et al.* Direction determination in the minus-end-directed kinesin motor ncd. *Nature* **395**, 813–816 (1998).
10. Kozielski, F., De Bonis, S., Burmeister, W. P., Cohen-Addad, C. & Wade, R. H. The crystal structure of the minus-end-directed microtubule motor protein ncd reveals variable dimer conformations. *Structure* **7**, 1407–1416 (1999).
11. Endow, S. A. & Waligora, K. W. Determinants of kinesin motor polarity. *Science* **281**, 1200-1202 (1998).
12. Chandra, R., Salmon, E. D., Erickson, H. P., Lockhart, A. & Endow, S. A. Structural and functional domains of the *Drosophila* ncd microtubule motor protein. *J. Biol. Chem.* **268**, 9005–9013 (1993).
13. Stone, D. B., Hjelm, R. P. J. & Mendelson, R. A. Solution structures of dimeric kinesin and ncd motors. *Biochem.* **38**, 4938–4947 (1999).
14. Lakkaraju, S. K. & Hwang, W. Hysteresis-based mechanism for the directed motility of the Ncd motor. *Biophys. J.* **101**, 1105–1113 (2011).
15. Kikkawa, M. *et al.* Switch-based mechanism of kinesin motors. *Nature* **411**, 439–445 (2001).
16. Parke, C. L., Wojcik, E. J., Kim, S. & Worthylake, D. K. ATP hydrolysis in Eg5 kinesin involves a catalytic two-water mechanism. *J. Biol. Chem.* **285**, 5859–5867 (2010).
17. Vinogradova, M. V., Reddy, V. S., Reddy, A. S., Sablin, E. P. & Fletterick, R. J. Crystal structure of kinesin regulated by Ca^{2+}-calmodulin. *J. Biol. Chem.* **279**, 23,504–523,509 (2004).
18. Yun, M., Zhang, X., Park, C.-G., Park, H.-W. & Endow, S. A. A structural pathway for activation of the kinesin motor ATPase. *EMBO J.* **20**, 2611–2618 (2001).
19. Hwang, W., Lang, M. J. & Karplus, M. Force generation in kinesin hinges on cover-neck bundle formation. *Structure* **16**, 62–71 (2008).
20. Rice, S. *et al.* A structural change in the kinesin motor protein that drives motility. *Nature* **402**, 778–784 (1999).
21. Khalil, A. S. *et al.* Kinesin's cover-neck bundle folds forward to generate force. *Proc. Natl Acad. Sci. USA* **105**, 19247–19252 (2008).
22. Vinogradova, M. V., Malanina, G. G., Reddy, A. S. & Fletterick, R. J. Structure of the complex of a mitotic kinesin with its calcium binding regulator. *Proc. Natl Acad. Sci. USA* **106**, 8175–8179 (2009).
23. Hallen, M. A., Liang, Z.-Y. & Endow, S. A. Two-state displacement by the kinesin-14 Ncd stalk. *Biophys. Chem.* **154**, 56–65 (2011).
24. Way, M., Pope, P., Gooch, J., Hawkins, M. & Weeds, A. G. Identification of a region in segment 1 of gelsolin critical for actin binding. *EMBO J.* **9**, 4103–4109 (1990).
25. Song, H. & Endow, S. A. Rapid purification of microtubule motor domain proteins expressed in bacteria. *BioTechniques* **22**, 82–85 (1997).
26. Huang, T.-G. & Hackney, D. D. *Drosophila* kinesin minimal motor domain expressed in *Escherichia coli. J. Biol. Chem.* **269**, 16493–16501 (1994).
27. Chandra, R. & Endow, S. A. Expression of microtubule motor proteins in bacteria for characterization in *in vitro* motility assays. *Meth. Cell Biol.* **39**, 115–127 (1993).
28. Otwinowski, Z. & Minor, W. Processing of X-ray diffraction data collected in oscillation mode. *Meth. Enzym.* **276**, 307–326 (1997).
29. Adams, P. D. *et al.* PHENIX: a comprehensive Python-based system for macromolecular structure solution. *Acta Crystallogr. D* **66**, 213–221 (2010).
30. Emsley, P. & Cowtan, K. Coot: model-building tools for molecular graphics. *Acta Crystallogr. D* **60**, 2126–2132 (2004).
31. Chen, V. B. *et al.* MolProbity: all-atom structure validation for macromolecular crystallography. *Acta Crystallogr. D* **66**, 12–21 (2010).
32. Pettersen, E. F. *et al.* UCSF Chimera--a visualization system for exploratory research and analysis. *J. Comput. Chem.* **25**, 1605–1612 (2004).
33. DeLano, W. L. *The PyMOL Molecular Graphics System.* (DeLano Scientific, 2002).
34. The CCP4 suite: programs for protein crystallography. *Acta Crystallogr. D* **50**, 760–763 (1994).

Acknowledgments

This study was supported by grants from the NIH (5 R01 GM046225) and March of Dimes Foundation (#1-FY07-443) to SAE. We thank Nadir Ijaz for performing motility assays of wild-type GST/Ncd and analyzing the data, F Jon Kull and Seok-Yong Lee for helpful comments on the structure and Rebecca Liu for initial steps in NcdG347D plasmid construction. Crystallization, screening, and data collection and processing were performed in the Duke University X-ray Crystallography Shared Resource (Nathan I Nicely, Director). Diffraction data were collected at SER-CAT (Southeast Regional Collaborative Access Team) at Argonne National Laboratory, supported by the US Department of Energy, Office of Science, Office of Basic Energy Sciences, under contract No. W-31-109-Eng-38.

Author contributions

HLL purified and crystallized protein, performed experiments, analyzed and processed data, and made figures; CWP provided advice for crystallization and directed the diffraction data collection and processing; SAE designed the study, performed experiments, interpreted results, made figures and wrote the manuscript.

Additional information

Supplementary information accompanies this paper at http://www.nature.com/scientificreports

Competing financial interests: The authors declare no competing financial interests.

License: This work is licensed under a Creative Commons Attribution-NonCommercial-ShareAlike 3.0 Unported License. To view a copy of this license, visit http://creativecommons.org/licenses/by-nc-sa/3.0/

How to cite this article: Liu, H-L., Pemble IV, C.W. & Endow, S.A. Neck-motor interactions trigger rotation of the kinesin stalk. *Sci. Rep.* **2**, 236; DOI:10.1038/srep00236 (2012).